# Development of Fabrication Technology for Low Activation Vanadium Alloys as Fusion Blanket Structural Materials

T. Nagasaka 1), T. Muroga 1), K. Fukumoto 2), H. Watanabe 3), M. L. Grossbeck 4), J. M. Chen 5)

1) National Institute for Fusion Science, Toki, Gifu 509-5292, Japan
2) Institute for Materials Research, Tohoku University, Sendai 980-8577, Japan
3) Research Institute for Applied Mechanics, Kyushu University, Kasuga 816-8580, Japan
4) Oak Ridge National Laboratory, Oak Ridge, TN 37831-6376, USA
5) Southwestern Institute of Physics, Chengdu 610041, China
e-mail contact of main author: nagasaka@nifs.ac.jp

**Abstract.** High purity vanadium alloy products, such as plates, wires and tubes, were fabricated from reference high-purity V-4Cr-4Ti ingots designated as NIFS-HEAT, by using technologies applicable to industrial scale fabrication. Impurity behavior during breakdown, and its effect on mechanical properties were investigated. It was revealed that mechanical properties of the products were significantly improved by the control of Ti-C, N, O precipitation induced during the processes.

## 1. Introduction

Vanadium alloys are promising candidates for fusion blanket structural materials, because of their low activation property, high temperature strength, high resistance to neutron irradiation and good compatibility with liquid lithium[1, 2]. Large scale melting is essential to establish fabrication technology for components of the blanket system. In the 18th conference in this series, it has been reported that 30 kg and 166 kg scale ingots designated as NIFS-HEAT were melted in a collaboration program between the National Institute for Fusion Science, Japanese universities, and industries[3]. One of the critical issues for the melting was to reduce the levels of interstitial impurities, such as C, N and O, which were well known to deteriorate mechanical and irradiation properties of vanadium alloys. The oxygen level in the NIFS-HEAT ingots was successfully reduced to 130-180 wppm, which is half the level of previous large ingots produced by the U. S. Department of Energy program[4, 5]. The carbon and nitrogen levels were kept at about 60 and 100 wppm, respectively. In the present paper, fabrication processes for various products, such as plates, wires and tubes, were developed to maintain the higher purity and to obtain good mechanical properties, after investigation on the optimum process parameters and microstructures.

## 2. Fabrication process for plates, wires and tubes

The fabrication processes for plate, wire and tube products of NIFS-HEAT-2 were shown in Fig. 1. Since vanadium alloy is very reactive with the air above 700 K, the ingots were canned into stainless steel before hot working, such as hot forging, hot isostatic pressing (HIP) and shaping. Plates of 26 mm in thickness were obtained through hot working at 1173-1473 K, resulting in 52-55 % reduction in area, followed by removal of the can and the cold rolling to 68-74 % reduction in thickness. The surface of the plates was kept clean during the working.

The 26 mm-thick plate was cold rolled further into plates of 6.6, 4.0, 1.9, 1.0, 0.5 and 0.25 mm in thickness. The wires of 8 mm and 2 mm in diameter were swaged at room temperature

from the 26 mm-thick and the 6.6 mm-thick plates, respectively. For tubing, the 26 mm-thick plate was recrystallized at 1273 K for 2 hr in a vacuum. The annealed plate was machined into two kinds of pipes with 25 / 19, or 10 / 7 mm in outer diameter / inner diameter (OD / ID). Larger pipes were cold-rolled by 3-directional rolling into tubes with 10 mm in outer diameter and 0.5 mm in wall thickness (ϕ10-0.5t), and the smaller into ϕ4.57-0.25t tube. During the 3-directional rolling, intermediate annealing at 1123 K for 1 hr was conducted after 1-3 pass each. The effects of final annealing temperature on the hardness and the microstructures were investigated at the temperature range from 673 – 1373 K. As a result, the reference final annealing condition was decided at 1273 K for 2 hr for the plates, the wires and the tube products[6]. Every annealing was performed in a vacuum, where the products were wrapped with Zr or Nb getter foils to avoid contamination with gaseous impurities, such as C, N and O. The products have been distributed for Round-Robin tests in universities and laboratories in Japan, US, China, Russia, Germany and Spain. The working degree after the hot working were summarized as Table 1. Table 2 shows the results of chemical analyses for the NIFS-HEAT products.

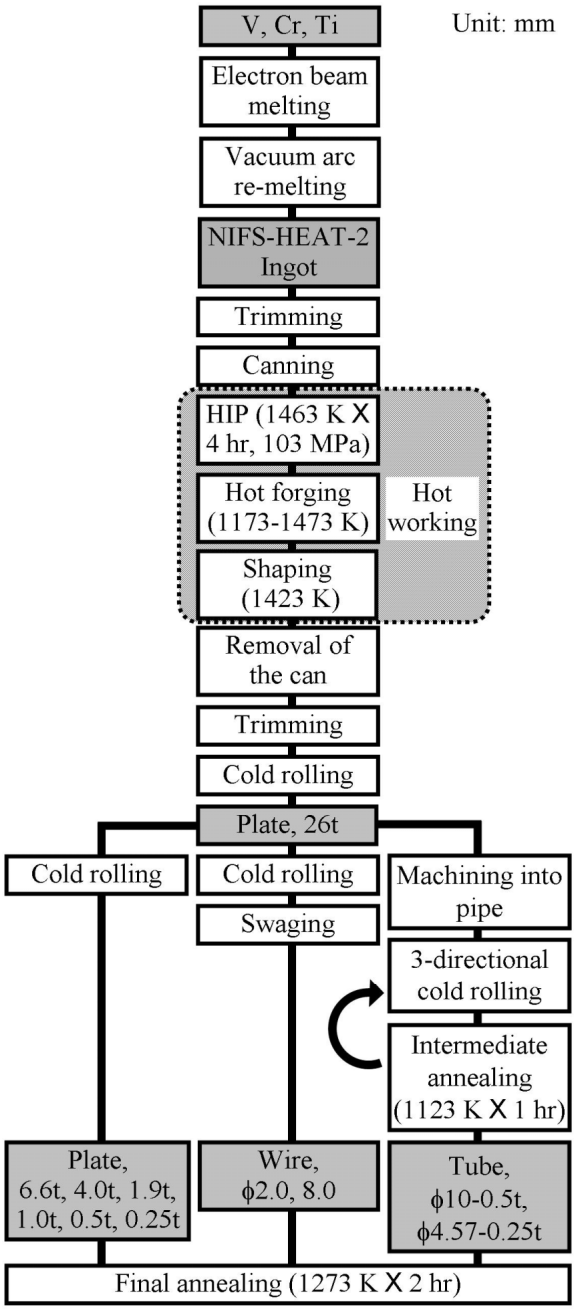


*FIG. 1 Fabrication process for the plate, wire and tube products of NIFS-HEAT-2.*

## 3. Evaluation procedure for the plates

The NIFS-HEAT plate products were evaluated by tensile tests, impact tests and microscopy. Tensile specimens were machined from the 26t, 4.0t and 0.25t plates after the final annealing at 1273 K X 2 hr. Gauge size of the specimen was 0.25 X 1.2 X 5 mm. Tensile tests were conducted with an initial strain rate of $6.7 \times 10^{-4}$ $s^{-1}$ at 300 K. In the impact tests, 1/3 size Charpy V-notch specimens (1/3 CVN) and 1.5 mm-square size specimens (1.5 CVN) were used. The specimen size / notch depth were 3.3 X 3.3 X 25.4 mm / 0.66 mm and 1.5 X 1.5 X 20 mm / 0.3 mm, respectively. The impact tests were performed after the final annealing with a cross head speed of 4.5 m $s^{-1}$ at 300 K and 77 K. Fig. 2 shows the definition of the position and the orientations of the specimens. For the 26t plate, homogeneity of the mechanical properties was investigated by the specimens from various positions in the thickness direction and with various orientations in

*Table 1 Working degree after hot working for the NIFS-HEAT products. The degree is defined as reduction in thickness for the plate products, whereas reduction in area for the wire and the tube products.*

| Products | Size (ID) / mm | Working degree, *R* / % |
|---|---|---|
| Plate | 26t | 74 |
| | 6.6t | 93 |
| | 4.0t | 96 |
| | 1.9t | 98 |
| | 1.0t | 99 |
| | 0.5t | 99.5 |
| | 0.25t | 99.8 |
| Wire | ϕ8 | 93 |
| | ϕ2 | 99.4 |
| Tube | ϕ10-0.5t | 93 |
| | ϕ4.57-0.25t | 92 |

*Table 2 Results of chemical analyses on impurities. (mass ppm, *mass %)*

| Product | Cr* | Ti* | H | C | N | O |
|---|---|---|---|---|---|---|
| Ingot / | 4.00 | 4.02 | | 50 | 96 | 122 |
| As-melted | 4.02 | 3.98 | | 69 | 122 | 148 |
| Plate 26t / As-rolled | 4.33 | 3.95 | 146 | 80 | 108 | 124 |
| Plate 26t / Annealed | 4.07 | 3.88 | 52 | 50 | 89 | 178 |
| Plate 4.0t / Annealed | | | 29 | 51 | 123 | 139 |
| Plate 0.25t / Annealed | | | | 62 | 84 | 158 |
| Wire ϕ2.0 / Annealed | | | 3.7 | 60 | 107 | 179 |
| Tube ϕ4.57-0.25t / Annealed | | | 4.5 | 120 | 120 | 330 |
| Tube ϕ10-0.5t / Annealed | | | 8 | 135 | 90 | 300 |

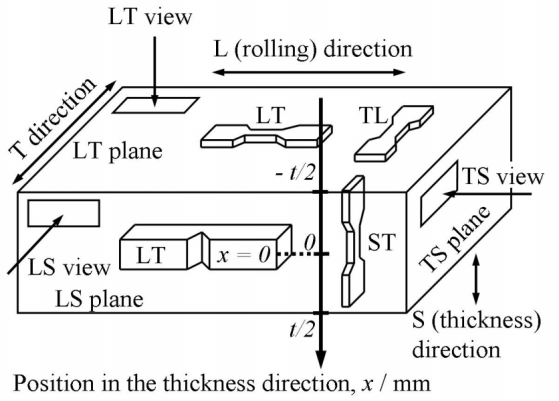


*FIG. 2 Definition of the specimen positions in the thickness direction and the orientation. For example, LT means that the specimen longitude is L direction and the crack for fracture propagates along to T direction. The axis for the position in the thickness direction, x, is taken along to the S direction. The origin for the position, x, is located at the center of the thickness, t. For example, x = 0 means that the center of the specimen is at the origin.*

the plate. The microstructures during the fabrication process and the fracture surfaces after the mechanical tests were characterized by transmission electron microscopy (TEM), scanning electron microscopy (SEM), energy dispersive X-ray analysis (EDX) and optical microscopy (OM).

## 4. Results

### 4.1. Orientation and position dependence of mechanical properties

Stress-strain curves for tensile tests are shown in Fig. 3. The specimens at $x = 0$ in all the orientations (dashed line curves) gave poor ductility as only 0.2 % in total elongation, whereas the near-surface specimens (solid line curves) at $x$ = -12.4 exhibited larger elongation than 10 %. Ductility was independent of specimen orientation, but dependent on the position in the thickness direction. Figure 4 shows load-deflection curves in the impact tests on the 26t plate. The load levels were similar to each other, while the load drop rate after the maximum load was slightly smaller for the specimen at $x$ = -12.4 mm, than that at $x$ = 0 and 12.4 mm. The specimen at x = -12.4 mm required larger load for crack propagation, and indicated larger absorbed energy, which is defined as the area enclosed by the load-deflection curve. Fig. 5 summarizes absorbed energy for the specimens at various positions in the thickness direction. In order to compare the absorbed energy among different size specimens, the energy is normalized with fracture volume parameter, which is given by $(Bb)^{3/2}$, where B is specimen width, 3.3 or 1.5 mm, and b is the ligament depth below the notch (width – notch depth), 2.64 or 1.2 mm, respectively[7]. The

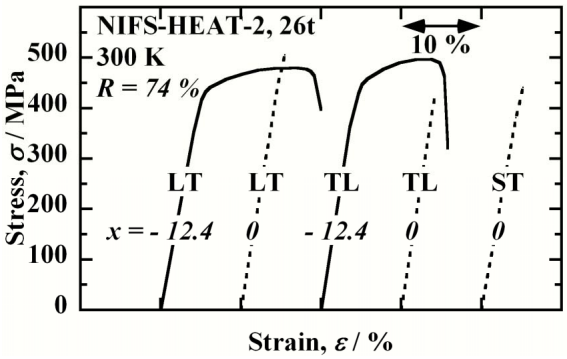


*FIG. 3 Stress-strain curves obtained in the tensile tests on the 26t plate. Specimen position, x, and orientations are indicated.*

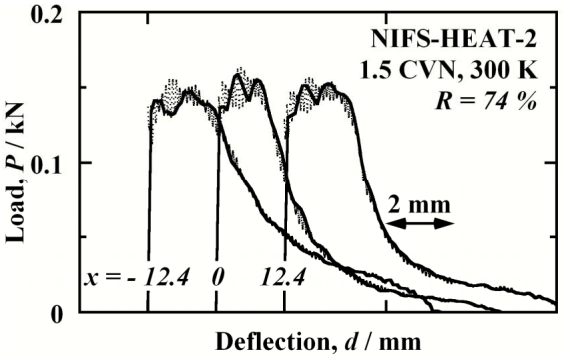


*FIG. 4 Load-deflection curves for the impact tests at 300 K.*

absorbed energy at 300 K around x = - 12.4 mm was higher than the other part, however the difference was not significant compared with the results of the tensile tests mentioned above. At 77 K, absorbed energy was reduced below half that at 300 K, but weakly dependent on the position in the thickness direction.

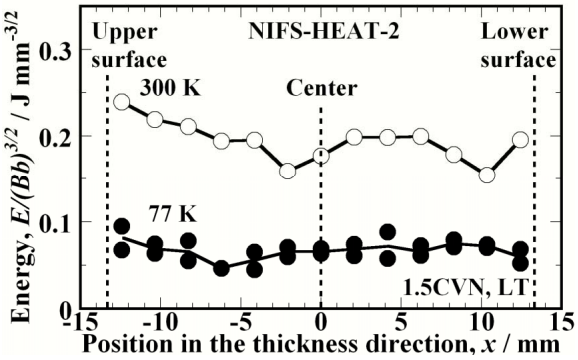


*FIG. 5 Absorbed energy in the impact tests on the 26t at 300 K and 77 K.*

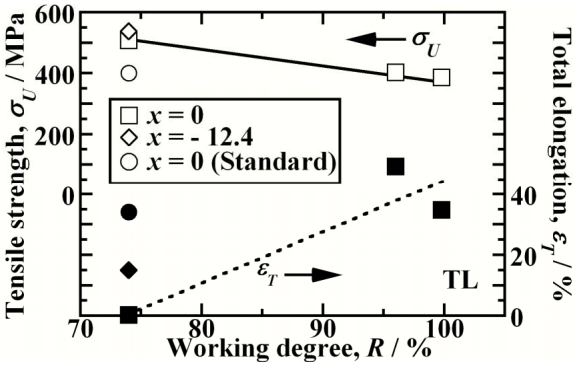


*FIG. 6 Change in strength and ductility by working. The lines were drawn after the data on the specimen at x = 0. Data for standard size specimen is referred from [8].*

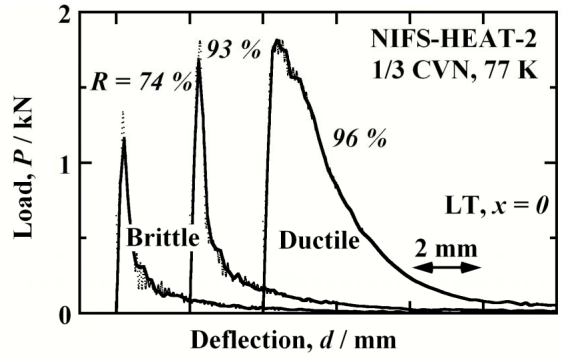


*FIG. 7 Load-deflection curves in the impact tests on the plates with various working degree.*

## 4.2. Improvement of mechanical property by further working

Tensile and impact properties of the plate were significantly improved by an increase in the degree of working. As shown in Fig. 6, tensile elongation for the TL specimen at $x$ = 0 mm was quite lower than that at $x$ = -12.4 mm. The elongation, however, increased with increasing working degree, $R$, accompanied by decrease in tensile strength. On the other hand, standard size (ϕ6.25 X 30 mm for the parallel part) specimen has shown lower strength and larger elongation even with low $R$[8].

Fig. 7 shows load-deflection curves in the impact tests at 77 K. The plates with $R$ = 74 % and 93 % showed brittle fracture, and poor absorbed energy of less than 0.054 J mm$^{-3}$. By the increase in $R$ up to 96 %, the fracture mode was changed to ductile, and the absorbed energy was improved to 0.17 J mm$^{-3}$. Fig. 8 summarizes the absorbed energies obtained in the impact tests with 1/3 CVN and 1.5 CVN at 300 K and 77 K.

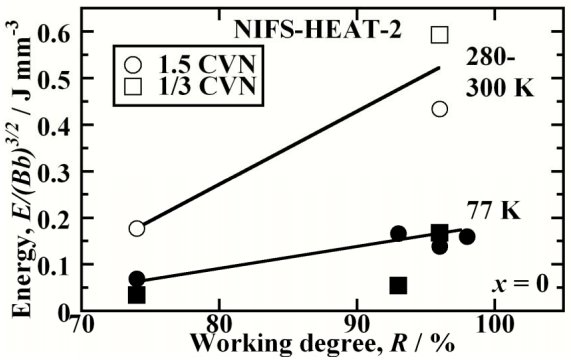


*FIG. 8 Improvement of absorbed energy by working.*

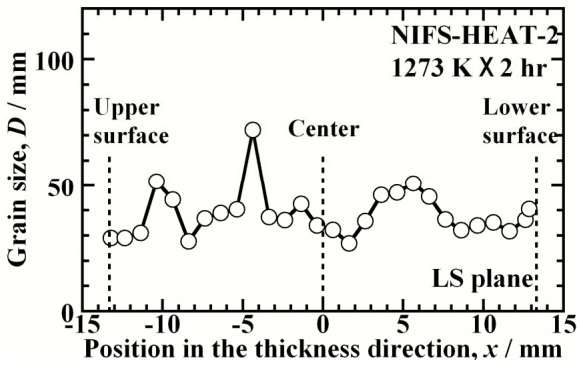


*FIG. 9 Grain size distribution in the 26t plate determined by OM observations.*

### 4.3. Orientation and position dependence of microstructures

Figure 9 shows grain size distribution in the 26t plate. The average grain size was 39 μm. No significant dependence of grain size on position was observed. From the SEM-EDX experiments, it was found that clusters of Ti-rich precipitates were produced during the hot working process. Fig. 10 shows the development of Ti-rich precipitates in the as-melted ingot by simulated annealing at the same temperature as hot working. In the as-melted ingot, no Ti segregation at the precipitates was detected. After annealing at 1273 K and 1423 K, clusters of Ti-rich precipitates were observed. The clusters of the precipitates were redistributed into precipitate bands aligned to the rolling direction with an increase in the degree of cold working, $R$. Fig. 11 shows the precipitate clusters and the bands in the 26t plate. Near the surface of the plates ($x$ < -8.4 mm), only the band structures were observed, while the precipitate clusters were observed as well as the bands around $x$ = 0 mm.

### 4.4. Effect of working on microstructures and fracture mode

In the plates of the 6.6 mm and thinner, where $R$ > 93 %, no cluster were but narrow and

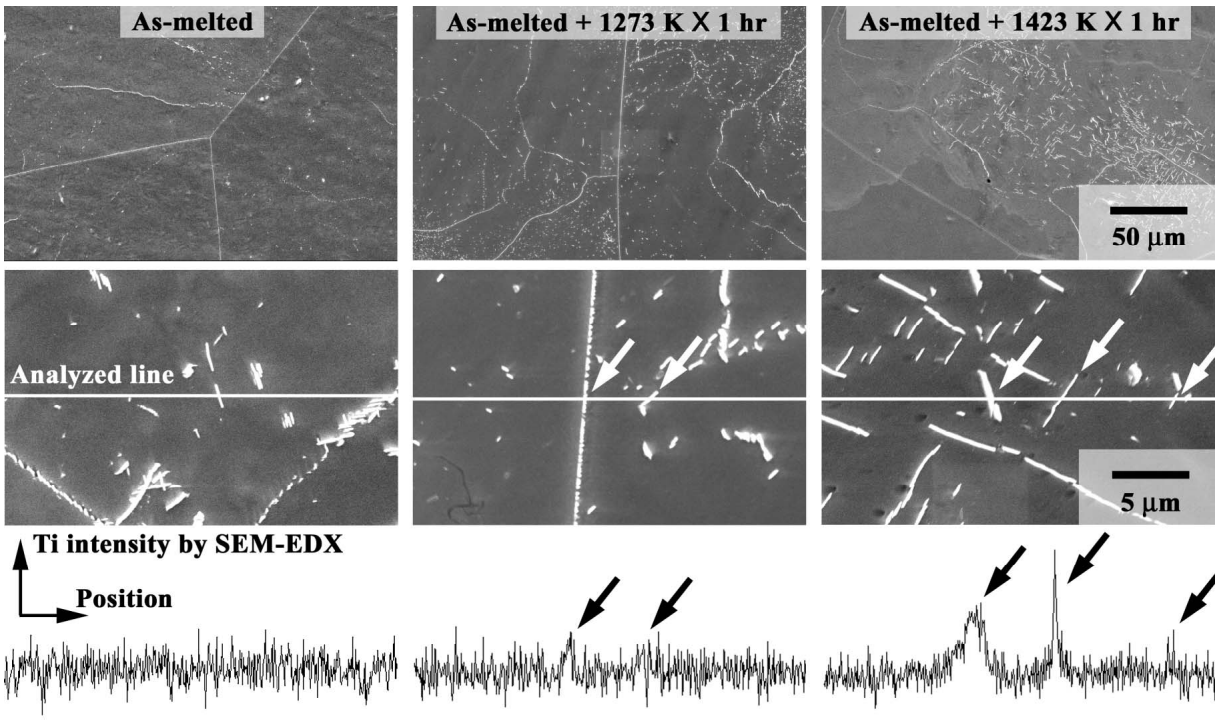


*FIG. 10 SEM images and Ti intensity by EDX of precipitates in the as-melted ingot and after annealing at the same temperature as the hot working. White and black arrows indicate Ti-rich precipitates and Ti peaks at SEM-EDX spectra, respectively.*

crowd bands were found. Fig. 12 shows typical band structures observed in the 4.0 mm-thick plate. Typical fracture surfaces after the impact tests were shown in Fig. 13. Secondary cracks were observed in all the specimens. In the plates with $R$ = 74 % and 93 % (26t and 6.6t), the secondary crack propagated to the random directions. On the contrary, the secondary crack in the plate with $R$ = 96 % and 98 % (4.0t and 1.9t) propagated along the precipitate bands.

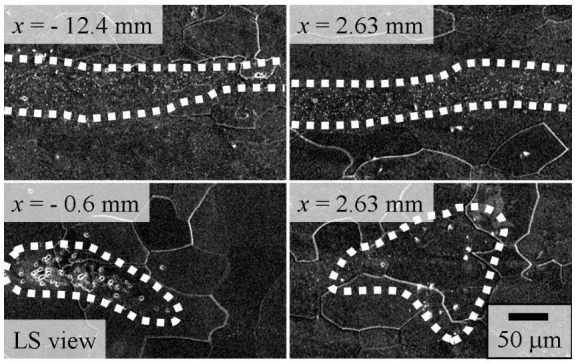


*FIG. 11 SEM images of Ti-rich precipitates in the 26t plate. Dashed lines indicate the bands (top) and clusters (bottom) of the precipitates.*

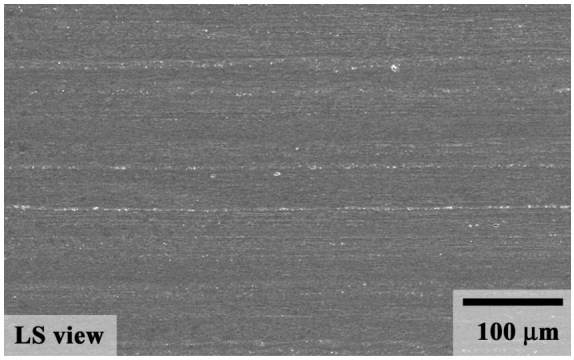


*FIG. 12 Band structures of Ti-rich precipitates along to the rolling (L) direction.*

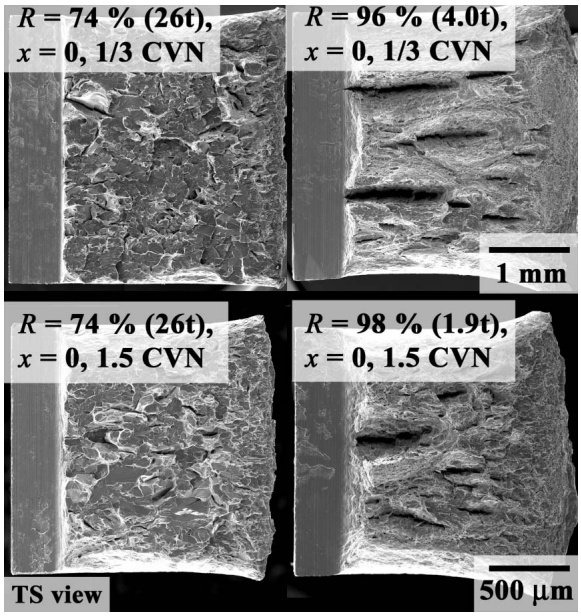


*FIG. 13 Fracture surfaces after the impact tests. Notch is located at the left side.*

## 5. Discussion

### 5.1. Impurity behavior in the fabrication process

In Table 2, impurity contaminations in the fabrication process can be estimated by the difference of the concentration in the products and that in the as-melted ingot. During the fabrication process, contaminations in the process except tubing were only 30, 33 and 56 mass ppm or less for carbon, nitrogen and oxygen, respectively. Hydrogen was removed by the vacuum annealing. The two kind of tube products were contaminated with 85 and 208 mass ppm of carbon and oxygen at the maximum, while nitrogen contamination was 24 mass ppm, which is similarly low to the other products. The additional contaminations of the carbon and oxygen are likely due to a number of intermediate annealing at 1123 K. Possible contamination sources are carbon, nitrogen, oxygen and their compound gases in the vacuum for annealing, and also the residual scale and lubricant on the surface of tube wall. Improvement of vacuum atmosphere and cleaning of the tube wall is required for getting further purity. It has been, however, reported that the ϕ4.57-0.25t tube did not show significant ductility loss and other mechanical property change[9]. Therefore the contamination level in the present fabrication process is acceptable and expected not to degrade the mechanical performance of NIFS-HEAT alloy. The NIFS-HEAT products maintain higher purity than previous work for the US DOE heat[4, 5]. Especially levels of oxygen in the plates and wires are half that in the US heat, so that superior weldability, irradiation resistance and so on are expected.

The Ti-rich precipitates observed in Fig. 10 are considered as Ti-C, N, O type precipitates common in V-Cr-Ti alloy[10, 11]. In the as-melted ingot, solidification and cooling rate was thought too high to produce the Ti-C, N, O precipitates, however supersaturated carbon was extracted out as vanadium carbide type precipitates because of relatively low solubility of carbon in vanadium matrix[12]. Above 873 K, mobility of Ti becomes high enough to react with the supersaturated C, N and O. The Ti-C, N, O precipitates are well known to appear from 873 K and above[11]. The hot working at 1173-1473 K was considered to evolve the Ti-C, N, O precipitates. The precipitates made clusters shown in Fig. 10 without working. In the fabrication process, the precipitates in the clusters were redistributed into bands under the deformation stress for working.

**5-2. Effect of oriented microstructure on mechanical properties**

In the impact tests, secondary crack are possibly initiated at the precipitate, and propagate to the nearby precipitate. In the clusters, a crack is thought to propagate to random direction, whereas it goes along the bands, if formed. Since the random directional crack shown in Fig. 13 seems easy to connect with each other, the clusters of the precipitates are thought to induce the brittle fracture, while the oriented and parallel cracks could not affect to the next cracks, and also could terminate the propagation of the primary crack. From Fig. 11, the size of the clusters was about 100 μm, which is comparable to 250 μm, the thickness of the miniature tensile specimens used in the present study, therefore the tensile elongation was very sensitive to the position, and was small around the area containing the precipitates clusters (around $x$ = 0). In Fig. 6, the standard size specimens has not shown such ductility loss, because the size of the parallel part, ϕ6.25 in diameter, was large enough relative to the cluster size. As shown in Fig. 11, precipitate band structures were observed near the surface of the 26t plate ($x$ < -8.4 mm), however they appeared much wavier compared with the thinner plate shown in Fig. 11. The wavy bands possibly cause the random directional cracks, and are considered to reduce absorbed energy at the thicker plates, as indicated in Fig. 4-8. From the results in Figs. 6 and 8, 74 % - 93 % seems to be a transition range for working degree from the brittleness to ductility. Working degree of 96 % is necessary for superior ductility both in the tensile and the impact tests.

In general, sufficient working to induce homogenization and recrystallization is necessary for improving ductility. Though the homogeneous grain structure was obtained as Fig. 9, mechanical properties significantly affected by the distribution of the Ti precipitates. In the case of vanadium alloys, it was revealed that sufficient working is critically required to obtain high ductility by the transition from precipitate clusters to bands.

**5.3. Tubing and welding processes**

It has been reported that the ϕ4.57-0.25t tube products had no precipitate clusters but precipitate bands aligned to the rolling direction[9]. The bunds, however, were wavier than that in the 0.25t plates. It was indicated that surface cracks of the tubes were induced at the intersection point between the bands and the surface and propagated along the bands. Recovery of work hardening by periodic intermediate annealing at 1123 K for 1 hr was crucial to reduce deformation stress and to prevent surface cracking. The resulting tubes exhibited good tensile strength and ductility comparable to the plates[9, 13].

Weld joints of 6.6 mm and of 4.0 mm-thick plates were fabricated by gas-tungsten-arc welding and laser welding in a high-purity Ar gas. Both the plates showed excellent

weldabilty[14, 15]. All the precipitates in the weld metal were dissolved during welding. The re-precipitation of Ti-C, N, O with high number density around 873 K resulted in significant hardening of the weld metal and degraded its impact properties[16, 17]. Post-weld heat treatment (PWHT) at 1073 K was effective to reduce the number density of the precipitates and hence to recover the hardening and the impact properties[17]. For vanadium alloy, several mm-thick plates have been suggested as components for blanket structural materials[18]. Based on the superior mechanical properties and weldability of the sufficiently worked plate, such as 4.0t plates, production of the several mm-thick plates and their structures are feasible by applying the fabrication process developed in the present study.

## 6. Conclusions

The present study revealed critical technologies and optimum process parameters for vanadium alloy products having superior mechanical performance. The mechanical properties of the products were improved significantly not only by reducing the impurity levels of C, N and O, but also by controlling density, size and distribution of the Ti-C, N, O precipitates. Thus the large scale fabrication of vanadium alloy products for fusion blanket is feasible with appropriate management of the process.

**Acknowledgement**

Authors are grateful to Prof. N. Noda in National Institute for Fusion Science and Dr. N. J. Heo in Center for Advanced Research of Energy Conversion Materials, Hokkaido University, the staff of International Research Center for Nuclear Materials Science, Institute for Materials Research, Tohoku University, for fruitful discussion and support in experiments.

**References**

[1] R. J. Kurtz, K. Abe, V. M. Chernov, D. T. Hoelzer, H. Matsui, T. Muroga and G. R. Odette, J. Nucl. Mater., **329-333** (2004) 47.
[2] Najmabadi et al., Fusion Eng. Des. **38** (1997) 3.
[3] T. Muroga and T. Nagasaka, FTP1/09, Proc. 18th Intl. Conf. Fusion Energy (IAEA CN-77) , Sorrento, Italy, Oct. 4-10, 2000.
[4] H. M. Cheng, B. A. Loomis and D. L. Smith, J. Nucl. Mater., **239** (1996) 139.
[5] W. R. Johnson and J. P. Smith, J. Nucl. Mater., **258-263** (1998) 1425.
[6] N. J. Heo, T. Nagasaka, T. Muroga, J. Nucl. Mater., **325** ( 2004) 53.
[7] W. R. Corwin and A. M. Hougland, “The Use of Small-Scale Specimens for Testing Irradiated Material”, Eds. W. R. Corwin and G. E. Lucas, ASTM-STP 888 (1986) 325.
[8] A. Nishimura, T. Nagasaka and T. Muroga,, J. Nucl. Mater., **307-311** (2002) 571.
[9] T. Nagasaka, T. Muorga and T. Iikubo, Fusion Sci. Technol., **44** (2003) 465.
[10] D. T. Hoelzer, Fusion Mater. Semiannual Progress Rep., DOE/ER-0313/25 (1998) 59.
[11] N. J. Heo, T. Nagasaka, T. Muroga and H. Matsui, J. Nucl. Mater., **307-311** (2002) 620.
[12] D. L. Harrod and R. E. Gold, Int. Met. Rev., **25** (1980) 163.
[13] K. Fukumoto, H. Matsui, M. Narui, T. Nagasaka and T. Muroga, J. Nucl. Mater,, **335** (2004) 103.
[14] T. Nagasaka, M. L. Grossbeck, T. Muroga and J. F. King, Fusion Technol., **39** (2001) 664.
[15] N. J. Heo, T. Nagasaka, T. Muroga, A. Nishimura, K. Shinozaki and H. Watanabe, Fusion Sci. Technol., **44** (2003) 470.
[16] T. Nagasaka, T. Muroga, M. L. Grossbeck and T. Yamamoto, J. Nucl. Mater., **307-311** (2002) 1595.
[17] N.J. Heo, T. Nagasaka, T. Muroga, H. Watanabe, A. Nishimura, K. Shinozaki, J. Nucl. Mater. To be published.
[18] L. A. El-Guebaly and the ARIES Team, Fusion Eng. Des. **38** (1997) 139.